nature communications

Article

https://doi.org/10.1038/s41467-024-51501-8

Microsecond triplet emission from organic chromophore-transition metal dichalcogenide hybrids via through-space spin orbit proximity effect

Received: 2 November 2023

Accepted: 7 August 2024

Published online: 02 December 2024

Check for updates

Jinho Choi[1,2,3,12], Healin Im[4,5,12], Jung-Moo Heo[3], Do Wan Kim[6], Hanjie Jiang[7], Alexander Stark[7], Wenhao Shao[7], Paul M. Zimmerman[7], Gi Wan Jeon[8], Jae-Won Jang[6], Euy Heon Hwang[9], Sunkook Kim[4,13] ✉, Dong Hyuk Park[1,2,13] ✉ & Jinsang Kim[3,7,10,11,13] ✉

Efficient light generation from triplet states of organic molecules has been a hot yet demanding topic in academia and the display industry. Herein, we propose a strategy for developing triplet emitter by creating heterostructures of organic chromophores and transition metal dichalcogenides (TMDs). These heterostructures emit microsecond phosphorescence at room temperature, while their organic chromophores intrinsically exhibit millisecond phosphorescence under vibration dissipation-free conditions. This enhancement in phosphorescence is indicative of significantly enhanced spin-orbit coupling efficiency through coupling with TMDs. Through detailed studies on these hybrids from various perspectives, we elucidate key features of each component essential for generating microsecond triplet emission, including 2H-TMDs with heavy transition metals and aromatic carbonyl with an ortho-hydroxy group. Our intriguing findings open avenues for exploring the universal applicability of fast and stable hybrid triplet emitters.

Metal-free purely organic materials showing room-temperature phosphorescence (RTP) have attracted much attention as a possible alternative to the organometallic phosphors due to their tuneable luminescent properties, large design window, more environmentally friendly constituent atoms, and economic production cost[1,2]. These purely organic phosphors (POPs) have been utilized for various applications, including biosensors[3–6], optical sensors[7,8], and organic light-emitting diodes (OLED)[9–12]. Accordingly, much effort has been made to establish molecular design strategies to achieve purely organic room-temperature phosphorescent materials. Three practical strategies have been identified and commonly used[13]. El-Sayed rule-satisfying aromatic carbonyl[7,14,15], heavy halogen atoms[8], and effective

[1]Department of Chemical Engineering, Inha University, Incheon 22212, Republic of Korea. [2]Program in Biomedical Science & Engineering, Inha University, Incheon 22212, Republic of Korea. [3]Department of Materials Science and Engineering, University of Michigan, Ann Arbor, MI 48109, USA. [4]School of Advanced Materials Science and Engineering, Sungkyunkwan University, Suwon 440-746, Republic of Korea. [5]Department of Materials Science and Engineering, University of California, Berkeley, CA 94720, USA. [6]Division of System Semiconductor, Dongguk University, Seoul 04620, Republic of Korea. [7]Department of Chemistry, University of Michigan, Ann Arbor, MI 48109, USA. [8]Particle Beam Research Division, Korea Atomic Energy of Research Institute, Gyeongju 38180, Republic of Korea. [9]SKKU Advanced Institute of Nanotechnology (SAINT), Sungkyunkwan University, Suwon 440746, Republic of Korea. [10]Macromolecular Science and Engineering, University of Michigan, Ann Arbor, MI 48109, USA. [11]Biointerfaces Institute, University of Michigan, Ann Arbor, MI 48109, USA. [12]These authors contributed equally: Jinho Choi, Healin Im. [13]These authors jointly supervised this work: Sunkook Kim, Dong hyuk Park and Jinsang Kim. ✉e-mail: seonkuk@skku.edu; donghyuk@inha.ac.kr; jinsang@umich.edu

https://doi.org/10.1038/s41467-024-51501-8

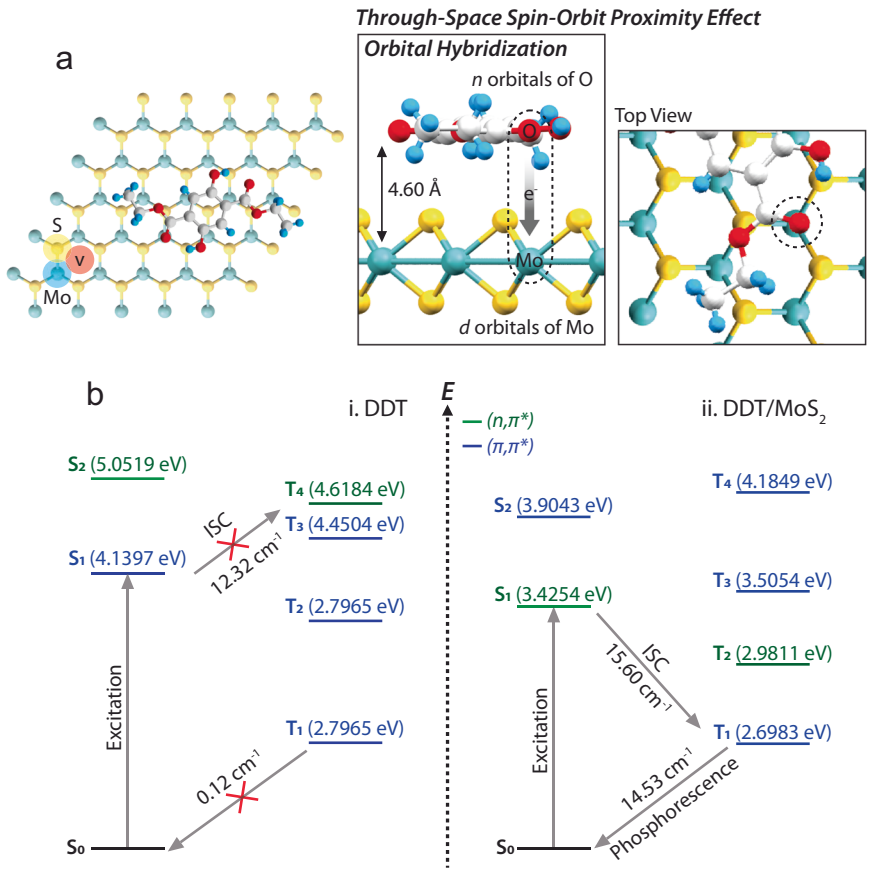

Fig. 1 | The through-space spin-orbit proximity effect of DDT/MoS_2. a Schematic illustration of the molecular arrangement of DDT on the MoS_2 basal plane, illustrating the microsecond RTP activation in the hybrid DDT/MoS_2 by leveraging the through-space spin-orbit proximity effect between the carbonyl oxygen and Mo atoms. **b** Excitation energy diagrams for both DDT molecule and DDT/MoS_2 system, along with the electron transition character for each excited state, calculated using the B3LYP functional. The SOC values of accessible ISC pathways are labeled, in units of cm^{-1}. (left) DDT molecule and (right) DDT/MoS_2 system. DDT, a purely organic emitter devoid of heavy atoms, exhibits fluorescence at RT. As solvents evaporate, DDT adsorbs onto the basal plane of MoS_2. In the DDT/MoS_2 heterostructure, MoS_2 triggers the enhanced SOCs and electron spin flipping of carbonyl oxygens at the excited states, facilitating efficient intersystem crossing and microsecond RTP.

suppression of molecular collisions[9,10,16]. For example, strong halogen bonding between electron-rich carbonyl moieties and electron-deficient halogens in purely organic phosphors can effectively restrict intermolecular collisions as well as implement the heavy atom effect to facilitate spin-orbit couplings (SOCs)[17]. POP guests in a rigid host matrix with strong intermolecular interactions can efficiently mitigate the vibrational decay of the embedded POPs[8,18,19]. While these approaches render bright RTP, the phosphorescence emission lifetime is pinned at milliseconds to a few seconds[8,20]. The long emission lifetime of POPs is attributed to the absence of heavy metal atoms and inevitably weak SOC. Even though the slow emission of POPs is feasible for sensing applications since the slow decay allows long enough time for POPs to respond to external stimuli or the presence of analytes, it is detrimental to light-emitting device applications in modern displays operating at a high frequency of up to 240 Hz. The emission lifetime of POPs should demand at least a microsecond regime to be practically applicable for OLEDs operating at more than 120 frames per second without the ghost effect of residual images. Moreover, a long emission lifetime inevitably causes the triplet-triplet anhelation issue due to accumulated triplet excitons. Thus, devising an effective, and generally applicable approach to vastly enhance the SOC of POPs is crucial from an electron spin dynamics perspective.

Contrastingly, organometallic phosphors, the prevalent triplet emitters, are composed of a heavy transition metal, such as iridium (Ir) and platinum (Pt), and organic ligands. The complex charge character of the coordination bonding between the transition metal and organic ligands is the origin of the phosphorescence generation. The heavy transition metals of organometallic phosphors effectively promote strong SOCs and render the fast phosphorescence emission in the microsecond regime, beneficial to OLED applications. However, during the device operation, dislocation of the metal from the organometallic framework causes material degradation and a significant decrease in brightness, particularly for blue phosphors, a critical and yet unsolved drawback of the organometallic phosphors[21].

Herein, we propose a strategy to realize ultrafast microsecond triplet emitters by hybridizing purely organic chromophores with transition metal dichalcogenides (TMDs) as schematically depicted in Fig. 1. Diethyl 2,5-dihydroxy terephthalate (DDT), a purely organic fluorophore, contains aromatic carbonyl groups associated with producing singlet and triplet states with (n,π^*) characters, possibly employing (n,π^*) to (π,π^*) intersystem crossing routes for triplet population[22]. DDT intrinsically emits ultralong phosphorescence in a millisecond regime at 77 K, a vibration-dissipation-free condition due to the weak SOCs attributed to the absence of internal heavy metal. Inspired by an external spin-orbit proximity effect of TMDs, where TMDs boost SOCs of adjacent two-dimensional (2D) materials in the vicinity by vertically stacking[23–25], we constructed heterostructures of DDT with various TMDs, e.g., MoS_2, $MoSe_2$, WS_2, and WSe_2, and observed the TMDs-induced photophysical variations in DDT. Surprisingly, DDT on TMDs emits bright green phosphorescence with a few tens of microsecond lifetimes at room temperature (RT). This reveals immensely enhanced SOCs of DDT via the through-space spin-

https://doi.org/10.1038/s41467-024-51501-8

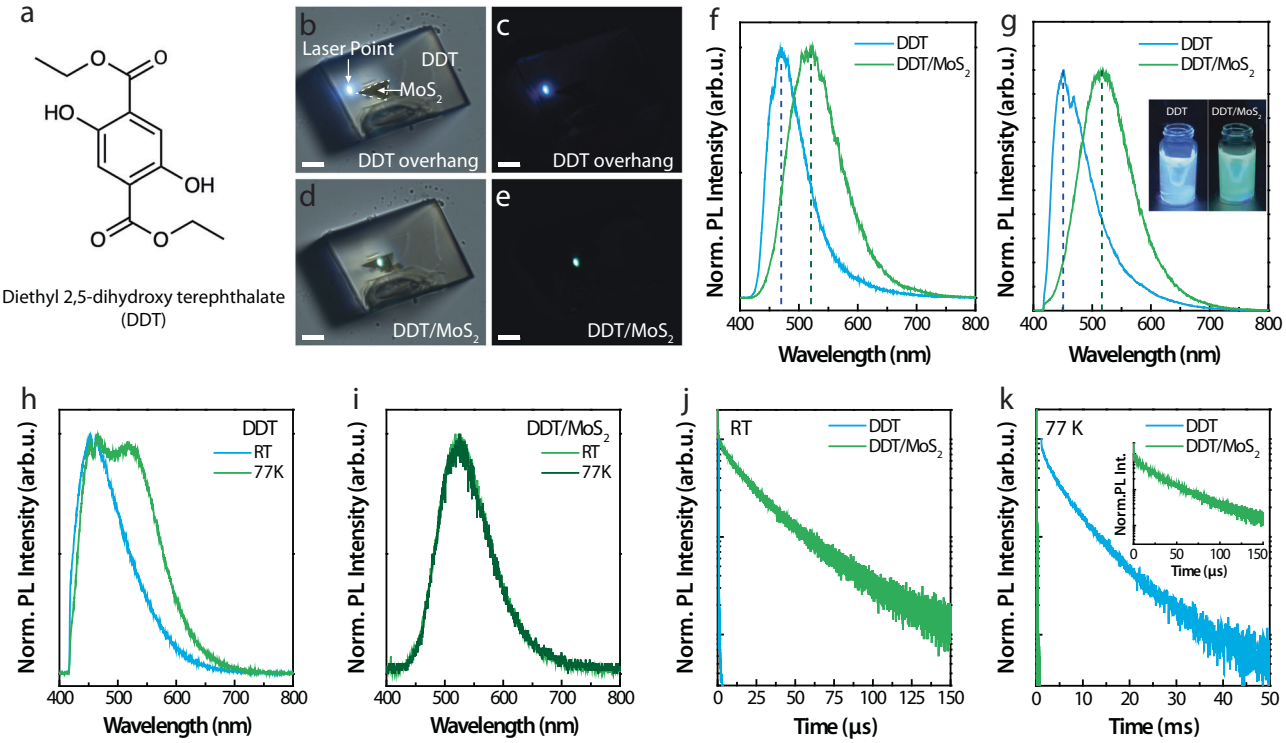

Fig. 2 | Photophysical properties of DDT and DDT/MoS_2. **a** Molecular structure of DDT. **b**–**e** Optical microscope images of DDT crystal grown on MoS_2 under 405-nm laser irradiation (scale bar = 5 μm). DDT crystal overlaid on MoS_2 (DDT/MoS_2) shows green emission while DDT crystal overhang outside of MoS_2 emits blue fluorescence. **f** PL spectra of DDT overhang and DDT/MoS_2. **g** PL spectra and photos of DDT aqueous suspension and DDT/MoS_2 aqueous suspension. **h** PL spectra of 1 mM DDT DMF solution. **i** PL spectra of DDT/MoS_2 aqueous suspension prepared by precipitating 1 mM DDT DMF solution into MoS_2 aqueous suspension. TRPL spectra of 1 mM DDT solution in DMF and DDT/MoS_2 aqueous suspensions at (**j**) RT and (**k**) 77 K.

orbit proximity effect of TMDs in the heterostructure. Additionally, it is uncovered that sulfur vacancies in TMDs contribute to the introduction of triplet ground states in DDT, alongside the through-space spin-orbit proximity effect.

Moreover, we demonstrated microsecond RTP emission from manually designed organic chromophores consisting of an aromatic carbonyl core with ortho-hydroxyl side chains and the extensively studied POP, 2,5-dihexyloxy-4-bromobenzaldehyde (Br6A) by building TMDs heterostructures. Contrary to the central role of heavy atoms in the organometallic phosphors, such as defining the bandgap and emitting color, in the developed hybrid POPs/TMD system, the transition metal of TMD solely exerts external magnetic torque and facilitates SOCs and intersystem crossing of POPs. This intriguing finding may offer a hybrid organic phosphor design for a class of fast and stable microsecond RTP emitters.

Results

Microsecond RTP of DDT/MoS_2

Figure 2a shows the molecular structure of DDT, consisting of an aromatic carbonyl core with hydroxyl side groups. DDT emits a few nanosecond blue fluorescence but no phosphorescence at RT[26]. For ease of fabrication, DDT was dissolved in dimethylformamide (DMF) at 1 mg/ml concentration and drop-cast on a Si/SiO_2 substrate having transferred MoS_2 flakes. As the solvent evaporates, DDT crystals are site-specifically formed on the MoS_2 flakes via the heterogeneous nucleation and growth mechanism as visualized in the in situ optical microscope images (Supplementary Figs. 1 and 2). DDT molecules reach and align on the MoS_2 basal surface, preferentially forming the heterostructure of DDT/MoS_2[27,28]. Bright (Fig. 2b and d) and dark (Fig. 2c and e and Supplementary Movie 1) field microscope images of DDT crystal on MoS_2 exhibit distinct colors when the laser excitation is focused on the overlaid (Figs. 2d and 1e) versus overhang (Fig. 2b and c) areas. Very intriguingly, the DDT crystal overlaid on MoS_2 (DDT/MoS_2) shows green emission, while the DDT crystal overhang outside of MoS_2 emits blue fluorescence. Accordingly, the photoluminescence (PL) spectra of DDT overhang and DDT/MoS_2 exhibit the maximum emission wavelength (λ_{em}) of 470 and 519 nm, respectively (Fig. 2f). The large 49 nm bathochromic shift of DDT/MoS_2 implies that MoS_2 exerts an additional external electromagnetic effect on DDT. The same phenomenon was also observed from the precipitated DDT in water and in an aqueous suspension of MoS_2 powders prepared by dropwise adding 1 mg/ml DDT/DMF solution into deionized water and the MoS_2 suspension (Fig. 2g and Supplementary Movie 2). λ_{em} of the solidified DDT and DDT/MoS_2 in aqueous solutions are 451 and 516 nm, respectively, consistent with the results from the DDT crystals grown on MoS_2 flakes. The emission quantum yields (QY) of the aqueous suspension of DDT and DDT/MoS_2 were measured in an integrating sphere to be 19 and 16 %, respectively.

We then investigated the latent phosphoresce of DDT at 77 K to understand the origin of its green emission on MoS_2. Phosphorescence from POPs having small SOCs is very slow at mostly milliseconds or longer. In addition, unless molecular motions of POPs are effectively engineered to be suppressed, non-radiative vibrational collision routes predominantly quench their phosphorescence. Thus, lowering the temperature to 77 K is the simplest effective way to freeze molecular motions and shut down the non-radiative vibrational collision routes[29,30]. Figure 2h shows the PL spectra of 1 mM DDT solution in DMF at RT and 77 K, respectively. While at RT, only the blue fluorescence peak is observed, at 77 K, a new green emission peak at 517 nm emerges along with the fluorescence peak, implying that triplet states and phosphorescence of DDT are activated by restricting the vibrational decay. Interestingly, as shown in Fig. 2i, the DDT/MoS_2 suspension shows essentially identical emission spectra at RT and 77 K, indicating that its phosphorescence is very fast so as to negate the non-

radiative decay routes at RT. Moreover, DDT/MoS_2 does not show even a trace of fluorescence, suggesting effective singlet to triplet intersystem crossing (ISC).

Time-resolved photoluminescence (TRPL) analysis was carried out for the 1 mM DDT solution and DDT/MoS_2 aqueous suspension at RT. As shown in Fig. 2j, the blue fluorescence emission of the DDT solution has an approximately 0.51 ns lifetime, whereas the green emission of the DDT/MoS_2 suspension shows a substantially longer lifetime of approximately 23.22 µs at RT. This suggests that the green emission of DDT/MoS_2 could be associated with a phosphorescent component, consistent with the low-temperature PL results. To compare the phosphorescence characteristics of DDT/MoS_2 with pristine DDT, the emission decay was measured on both pristine DDT and DDT/MoS_2 at 77 K. Under such extremely low-temperature conditions, where thermal energy is nearly zero, the collisional loss of non-radiative transition is minimized, allowing the emergence of the intrinsic phosphorescence that is otherwise undetectable at RT. The intrinsic phosphorescence of the DDT solution exhibits a notably long lifetime of 4 ms at 77 K due to the weak SOCs, similar to other POPs (Fig. 2k). However, DDT/MoS_2 maintains a microsecond-scale phosphorescence of 27.98 µs at 77 K, indicating its phosphorescent emission is already activated at RT. It's worth noting that the phosphorescence lifetime of DDT/MoS_2 is about a few thousand times faster than DDT at 77 K, testifying explosively enhanced SOCs by MoS_2.

We also conducted additional TRPL analysis on the DDT crystal grown on the MoS_2 surface by shifting the excitation laser focus along Z-axis (Fig. 3a). When the laser was focused near the interface between DDT and MoS_2 (i), 17.95 µs of phosphorescence was obtained. In contrast, when the focus was off from the MoS_2 surface and reached the upper surface of the DDT crystal (ii) instead, only blue fluorescence with a 22.70 ns lifetime was measured. This reveals that the proximity from the MoS_2 contact surface influences the degree of enhancement in SOCs of DDT. Thus, the observed phenomena consistently point to the spin-orbit proximity effect of MoS_2 on organic molecules.

Raman analysis was performed to investigate the vibrational characteristics of the carbonyl of DDT and DDT/MoS_2. As aforementioned, carbonyl oxygens of DDT are a crucial component to possibly promote ISC routes associated with electron spin flipping along $(\pi,\pi^*) - (n,\pi^*)$ transition. We presumed that a strong interaction between carbonyl oxygens and MoS_2 would be inevitable for MoS_2 to turn on the phosphorescent emission of DDT. Figure 4a presents the Raman spectra of DDT and DDT/MoS_2 shown in Fig. 2b and d. As for

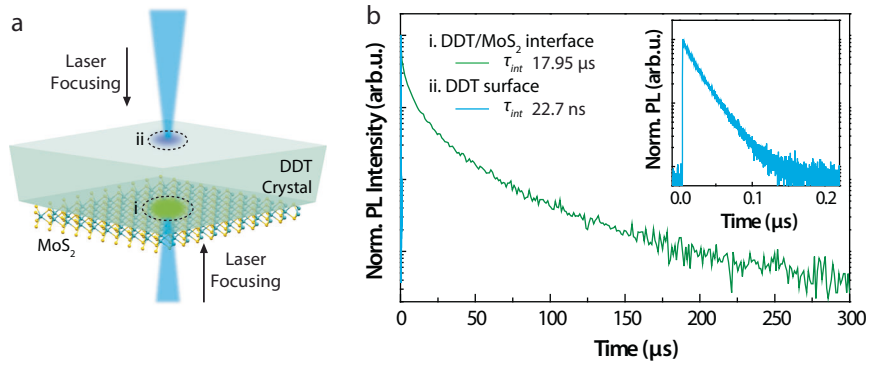

Fig. 3 | Photophysical properties of DDT/MoS_2 interface and DDT surface. a Experimental scheme and **b** TRPL spectra of DDT/MoS_2 interface and DDT surface at RT.

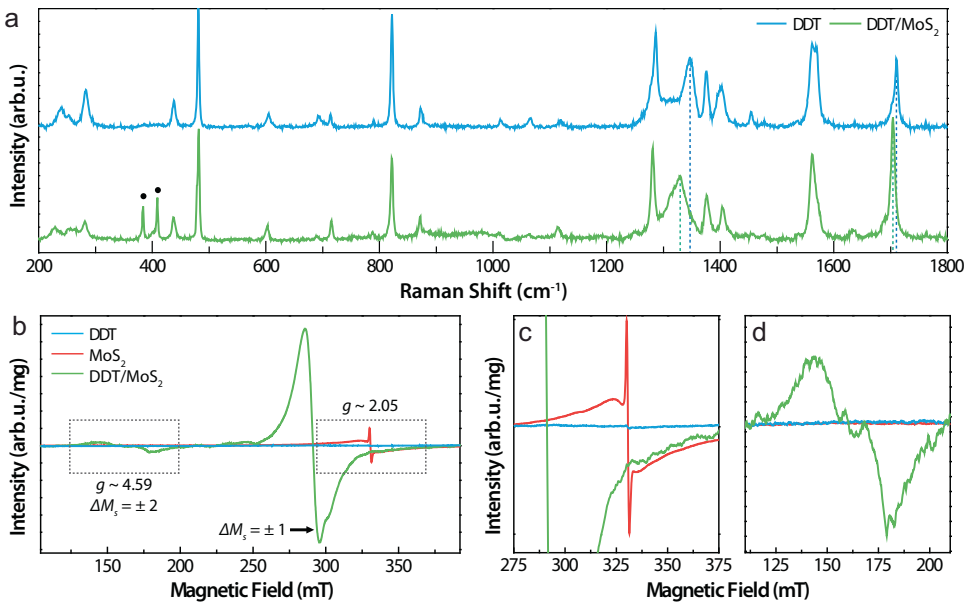

Fig. 4 | Raman and EPR spectra of DDT and DDT/MoS_2. a Raman spectra of the DDT overhang and DDT/MoS_2 interface of the DDT/MoS_2 structure shown in Fig. 2b and d. Black dots represent Raman modes of MoS_2. **b** X-band EPR spectra of DDT, MoS_2, and DDT/MoS_2 at RT under dark conditions. The magnification of the EPR peak of MoS_2 and half-field EPR transition in the range of (**c**) 275-375 mT and (**d**) 110-210 mT, respectively.

DDT, the peak at 1710 cm^{-1} represents the stretching modes of C = O bonds[31,32]. Notably, when combined with MoS_2, this peak shifts to a lower frequency region at 1704 cm^{-1}. In addition, the prominent peak obtained from pristine DDT at 1350 cm^{-1}, corresponding to C-O single bonds of DDT, also shows a blue shift to 1328 cm^{-1} in the presence of MoS_2. These variations may indicate energy loss of phonons and distorted electronic conformation within DDT crystals on MoS_2. It is likely associated with the El-Sayed rule, indicating a significant interaction between the carbonyl group of DDT and MoS_2 in DDT/MoS_2 heterostructures. The two new peaks at 409 and 384 cm^{-1} in DDT/MoS_2 correspond to A_{1g} and E^1_{2g} modes in multilayer MoS_2 (marked as dots)[33].

Thus far, we observed that MoS_2 could strengthen SOCs of DDT in an interfacial proximity manner to promote microsecond RTP by forming a heterostructure, and the carbonyl oxygen could be likely involved in that. Next, we tried to verify the electron spin dynamics of the DDT/MoS_2 hybrid system and gain experimental evidence to generate a microsecond RTP. SOCs are related to electromagnetic angular momentum changes attributed to specific magnetic torques from an external magnetic field and nuclear spin or orbital configuration changes, leading to electron spin flipping and ISC. Electron paramagnetic resonance spectroscopy (EPR) analysis is a well-known means to characterize the magnetic dipole moment (spin angular momentum) of electrons, offering information on the allowed and forbidden transitions.

The Continuous-Wave EPR (X-band) analysis on DDT, MoS_2, and DDT/MoS_2 was conducted under dark conditions (Fig. 4b). DDT powder has no distinguishable EPR signal. MoS_2 powder exhibits a typical EPR signal near 330 mT with an axially anisotropic g-factor (g ~ 2.05), as shown in Fig. 4c. Such EPR signal of MoS_2 can be ascribed to the defects coordinated with sulfur (thio-Mo^{5+}) located at low symmetry edge sites[34–37]. Interestingly, DDT/MoS_2 exhibits two EPR peaks unobserved in pristine DDT: a prominent peak at near 300.5 mT and a relatively small peak at 160 mT. The peak at 300.5 mT is associated with the allowed transition ($\Delta m_s = \pm 1$). The peak at 160 mT originates from the forbidden transition ($\Delta m_s = \pm 2$), known as the half-field transition of the triplet state[38–41]. The half-field transition is generally forbidden but has been reported in some systems with photo-excited or thermally excited triplet states[38,39,42]. The allowed transition at 300.5 mT is relatively narrow compared to reported EPR spectra[38,42–44]. In addition, it has been reported that the general linewidth of the forbidden transition is narrow, and the intensity is much smaller than the allowed transition because it is not broadened by the zero-field splitting[42–44]. However, in our observation, the half-field transition is fairly broad and relatively high compared to previous reports[38,42,45]. These newly emerging EPR signals of DDT/MoS_2 are most likely linked to triplet ground states[46,47] of DDT promoted by the proximity to MoS_2, as the measurements were carried out under dark conditions.

Then, we extracted *g*-factors from individual EPR signals in DDT/MoS_2. The half-field transition of DDT/MoS_2 at 160 mT exhibits a high g-factor up to approximately 4.59 (Fig. 4d), whereas the allowed transition of DDT/MoS_2 at 300.5 mT presents a g-factor of 2.25. The variation in the g-factor ($\Delta g = g\text{-}g_e$, where g and g_e are g-factors of the investigated materials and free-electron, respectively) is correlated to the spin-lattice relaxation time, T_1, attributed to SOC following the $T_1 \propto (\Delta g)^{-2}$ dependency[40]. Δg of DDT/MoS_2 is approximately 0.25, considerably larger than S- or Se-including organic semiconductors[40], implying that enhanced SOCs of DDT/MoS_2 lead to a short relaxation time, i.e., T_1 in a few nanoseconds scale. A short T_2 (spin-spin relaxation time) of 3.5 ns could also stem from the strong SOC of DDT/MoS_2 (Supplementary Fig. 3)[48].

Furthermore, light EPR (L-EPR) was carried out on DDT/MoS_2 under 375 nm laser irradiation. Notably, no EPR signals corresponding to excited triplet states of DDT were observed under these conditions (Supplementary Fig. 4). It may be attributed to the rapid spin relaxation derived from significantly enhanced SOC in the DDT/MoS_2 system. This is consistent with a recent study[49] where only long-lived spin-polarized states, such as polarons, are detectable in L-EPR. Instead, the overall intensity of EPR signals in DDT/MoS_2 is slightly reduced under light conditions. The light-induced population of excited triplet states may restrict triplet ground state populations in DDT/MoS_2.

Despite the inability to detect excited triplet states with L-EPR due to experimental limitations, distinct EPR signals are observed in DDT/MoS_2 compared to pristine DDT, and they are associated with triplet ground states in DDT as solid evidence of the enhanced SOCs of DDT/MoS_2. In addition, relatively large Δg extracted from each EPR signal also implies the possibility of ultrafast spin relaxations in DDT/MoS_2. Thus, it is experimentally proved that MoS_2 donates triplet characters through enhancing the SOCs of DDT, and promotes subsequent fast decay. From now on, we will term this phenomenon the through-space spin-orbit proximity effect of MoS_2 on DDT.

Through-Space Spin-orbit proximity effect of MoS_2 on DDT

To further understand the dynamics and driving forces of the through-space spin-orbit proximity effect of MoS_2 on DDT, information about how DDT molecules coordinate on the MoS_2 basal plane should be provided. Mo and S atoms of MoS_2 form honeycomb structures on the plane with broken inversion symmetry. As the number of layers increases, MoS_2 sheets are out-of-plane stacked by van der Waals (vdW) interaction. Most importantly, MoS_2 physically interacts with and attracts other organic molecules or 2D materials at its surface. At the interfacial attraction between organic materials and MoS_2, their binding affinities depend on the molecular structures and functional groups[50–52]. Internal affinity features in organic materials could lead to particular self-assembly or coordination of organic materials on the MoS_2 basal plane to stabilize the system at the lowest surface energy. This generates a few nm-spacing between them, facilitating charge transfer and orbital hybridizations. In DFT calculations, the binding energy between DDT and MoS_2 is approximately 0.194 eV, much larger than the Boltzmann energy of 0.026 eV at RT. Thus, due to the intense binding energy, once DDT molecules reach and attach to the MoS_2 basal plane, they are unlikely to part with each other.

We performed scanning tunneling microscopy (STM) analysis and vdW-corrected DFT calculation of DDT/MoS_2 to understand the structure and excited state dynamics of DDT with and without MoS_2. For STM analysis, scalable MoS_2 was synthesized by the reported two-step growth method and transferred on a 2D layered HOPG substrate by the hydrofluoric acid-assisted solution process[53]. 1 mg/ml DDT DMF solution was then dropped on the prepared MoS_2 to form DDT/MoS_2 for STM analysis utilizing a Pt/Ir STM tip. As shown in Supplementary Fig. 5, DDT molecules assemble as 2D layer-like structures on the MoS_2 basal plane. The center-to-center lateral intermolecular distance between DDTs is approximately 1.2 nm (corresponding to the length of 4 MoS_2 unit cells) and is highly uniform over a 400 nm2 area. Since MoS_2 synthesized by the two-step growth method comprises a few nm-scale grains forming amorphous structures, this result indicates that intermolecular interactions between DDT molecules themselves primarily govern their self-assembly into the 2D layer structure after the initial preferential adsorption of DDT at a particular site of the MoS_2 unit cells.

Furthermore, we conducted computational analysis based on the STM results to validate the alignment of DDT on the MoS_2 basal plane and to compute the total energy required for the formation of a stable heterostructure. This calculation could provide insight into the most stable alignment of DDT/MoS_2, allowing for an in-depth investigation into the detailed mechanism behind the through-space spin-orbit proximity effect of MoS_2 on DDT. Assumptions regarding the relative coordinates of DDT/MoS_2 are as follows; Firstly, the center of the phenyl ring of DDT serves as the reference point for DDT

(Supplementary Fig. 6a). Secondly, three potential binding sites on the MoS_2 basal plane were defined for the reference point of DDT to occupy: Mo atom, S atom, or the void of the MoS_2 honeycomb structure, as shown in Fig. 1a and Supplementary Fig. 6b. Lastly, potential coordinates of DDT on MoS_2 were selected as periodic self-assembles on 4 × 4 and 4 × 5 MoS_2 unit cells, denoted as DDT-r and DDT-t, respectively (Supplementary Fig. 6c and d). The alignments were obtained from the single-crystal XRD results of pristine DDT and DDT/MoS_2. Intriguingly, the crystal structure of DDT undergoes deformation from orthorhombic (symmetric alignment) to triclinic (asymmetric alignment) when coupled with MoS_2 during the crystallization process. Detailed crystallographic information and relevant descriptions are shown in Supplementary Fig. 7.

Supplementary Table 1 presents the total binding energy of DDT and MoS_2 depending on the DDT arrangements. The most stable alignment of DDT on the MoS_2 basal plane turned out to be the DDT-t on S atoms with the total energy of −22741.840 eV (Fig. 1a). In this alignment, most electrons are accumulated on carbonyl oxygen, and the carbonyl oxygen is aligned right above a Mo atom with the smallest spacing of 4.6 A.

As pointed out in recent reports[54], the key to maximizing the heavy atom effect in POPs is to enhance the involvement of a heavy atom's electrons in the orbital angular momentum transition of POPs, resulting in efficient SOC processes. In this regard, the close proximity between the heavy Mo atom and carbonyl oxygen in the heterostructures allows the electrons of Mo to readily interfere in the orbitals of DDT and subsequently participate in the SOC processes. This is highly essential for Mo atoms to efficiently prompt the through-space spin-orbit proximity effect of MoS_2 on DDT. Another important consideration is the hybridization potential of orbitals and the resultant extra magnetic torque. The broken inversion symmetry of MoS_2 provokes the valence-band-edge state to split the *d* orbitals of Mo atoms and completely decouple spin components, i.e., the spin-up (↑) at *K* point and spin-down (↓) at *K′* point, respectively[23,55]. This might destabilize the energy states and electron spin movements of DDT. In addition, the *d* orbitals of Mo atoms in MoS_2 and the *p* orbitals of carbonyl oxygen in DDT could influence each other to hybridize orbitals and exert an extra torque. Apart from that, anion-antisite defects in TMDs warrant further investigation, as they promote paramagnetic triplet ground states, and these features are preserved even in superlattice structures[56,57]. All these effects likely contribute to the through-space spin-orbit proximity effect in the DDT/MoS_2 hybrid system.

To computationally verify the through-space spin-orbit proximity effect of MoS_2 on DDT, further quantum chemical simulations were performed on a) the DDT molecule and b) a representation of the DDT/MoS_2 hybrid system, where in the latter, the MoS_2 surface is truncated to a single Mo unit (see computational details for a full description). Based on the above model, DDT and single-unit MoS_2 were separated at an intermolecular distance of 4.6 Å. Thus, the truncated DDT/MoS_2 system is a minimal model for quantum mechanical interactions between the surface and molecule. Excited state energies and SOC values are presented in Fig. 1b, and canonical orbitals demonstrating energy decrease of the (n, π*) transition are in Supplementary Fig. 9. Figure 1b shows that while most low-lying excited states in DDT, including S_1, T_1, and T_2, have (π, π*) character, T_3 of DDT is an (n, π*) state. T_3 is connected to the (π, π*) S_1 state through a significant SOCME (14.4 cm^{-1}), but T_3 sits ~0.84 eV above S_1, which makes it inaccessible for ISC from S_1. Importantly, since the SOC constant between the lowest excited triplet state T_1 to ground state S_0 is 0.4 cm^{-1}, the phosphorescence emission lifetime of DDT alone is expected to last long. These results are consistent with the time-resolved photoluminescence (TRPL) analysis, which showed in the previous section that intrinsic phosphorescence at DDT has a considerably long lifetime of 4 ms at 77 K.

Upon coordination of DDT to MoS_2, the (n, π*) excited states drop lower in energy, while the (π, π*) states stay in similar energetic positions. Due to this change, the singlet (n, π*) state of DDT becomes S_1 with MoS_2 present, and the T_3 (n, π*) state becomes T_1. This rearrangement in state order significantly affects excited state relaxation, as discussed in the following. The effect stems from raising the n, n′ orbital energy levels for DDT in the presence of MoS_2 (Supplementary Fig. 9), which enhances the charge transfer character of the (n, π*) states while reducing their excitation energy. The intensified charge transfer within DDT's excited states is, in turn, supported by charge transfer from MoS_2 (Supplementary Table. 3). The π orbitals are less affective of MoS_2 (Supplementary Fig. 10) and do not change as dramatically in energy as the free DDT molecule. This state reordering in DDT/MoS_2 provides feasible ISC pathways that were not viable for the free DDT molecule. As shown in Fig. 1b, the SOC between (n, π*) S_1 and (π, π*) T_2 state increases to 17.8 cm^{-1} with the presence of MoS_2, and the transition from (n, π*) S_1 to (π, π*) T_2 is downhill. This pathway accesses the triplet manifold, where internal conversion relaxes the (π, π*) T_2 state to the (n, π*) T_1 state. From T_1, phosphorescence yields the ground state S_0 through another newly accessible ISC pathway. Note that the DDT/MoS_2 heterostructure provides a T_1 - S_0 SOC of 62.3 cm^{-1}, two orders of magnitude larger than that of the free DDT molecule (0.4 cm^{-1}). This significant difference in T_1 - S_0 SOC suggests that MoS_2 exceedingly triggers the phosphorescence of DDT, as the rate of ISC is expected to scale with SOC squared – giving several orders of magnitude of fast decay speeds. This finding is also consistent with the experimental result, where the RTP lifetime of DDT/MoS_2 is about a few thousand times faster than DDT.

Figure 1a illustrates the microsecond RTP of DDT via the through-space spin-orbit proximity effect of MoS_2. Blue fluorescent DDT approaches and tightly adheres to the MoS_2 basal plane. One of the two carbonyl oxygens in DDT closely aligns on Mo atoms since DDT tends to assemble the most stable arrangement on the MoS_2 basal plane, where the phenyl center sits at S atoms. At this heterojunction, the close proximity of carbonyl oxygen and Mo atoms facilitates interfacial interactions between the *d* orbitals of MoS_2 and the *p* orbitals of carbonyl oxygen of DDT. Since, in MoS_2, broken inversion symmetry with strong SOCs and spin splits lowers the energy gap in the (n, π*) transition of DDT, the excited states of DDT/MoS_2 are reordered, promoting a new feasible ISC route (S_1-T_2) and significantly enhanced ratio of T_1 - S_0 SOC (62.3 cm^{-1}). Thus, it could be well interpreted that the presence of MoS_2 promotes a faster phosphorescence relaxation time than its intrinsic properties via the through-space spin-orbit proximity effect. Note that the calculations were conducted assuming a perfect lattice structure of the MoS_2 basal plane, with no defects.

Next, we examine the case of actual TMDs with sulfur vacancies in the DDT/MoS_2 heterostructure. In reality, defects in TMDs are unavoidable, although their concentrations per area may vary depending on preparation methods. Among these defects, sulfur vacancies are particularly intriguing as they behave as a magnetic moment or torque that is preserved even within a heterostructure[56,57]. It is investigated how triplet ground states stemming from MoS_2 influence the photophysical dynamics of the heterostructure. As aforementioned, pristine MoS_2 exhibits an EPR signal associated with anion-antisite defects, and surprisingly, the heterostructure also shows new EPR signals indicative of triplet ground states.

To understand this, computational analysis on the spin density of MoS_2 and DDT/MoS_2 was conducted, modeling sulfur defects as a high-spin triplet state on a 2 × 2 MoS_2 surface with one sulfur removed while keeping the system neutral. The defective MoS_2 initially owns a perfect spin density of 2 e^-. In the heterostructure, however, the spin density splits into 1.99 e^- on MoS_2 and 0.009 e^- on DDT, indicating significant electronic coupling likely causing the triplet ground states observed in dark EPR measurements. Based on this calculation, it is

https://doi.org/10.1038/s41467-024-51501-8

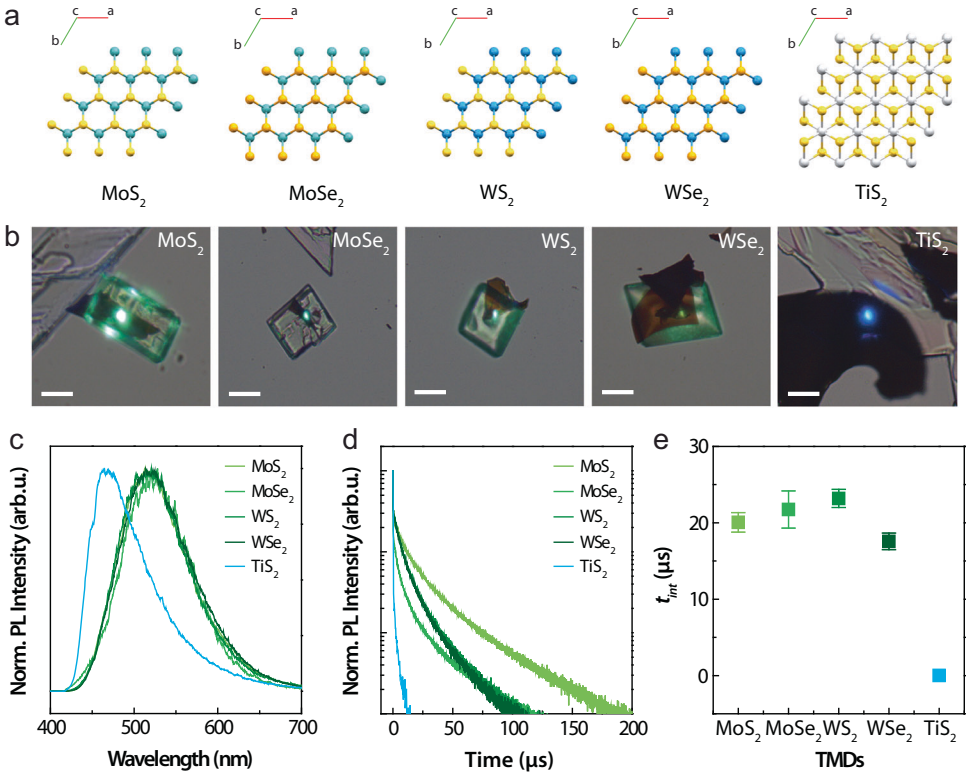

Fig. 5 | The through-space spin-orbit proximity effect of general TMDs on DDT. a Crystal structures of MoS_2, $MoSe_2$, WS_2, WSe_2, and TiS_2. **b** Optical images (scale bars = 10 μm), (**c**) PL, and (**d**) TRPL spectra of DDT/TMDs. **e** Statistics of average phosphorescent lifetimes with error bars for 10 samples of each DDT/TMDs composition.

reasonable to infer the radiative transition can occur through a triplet-to-triplet allowed transition when triplet ground states are present. This may also influence subsequent lifetime as well as excited states.

Attempts to compute energy band diagrams of DDT/MoS_2 with triplet ground states were made, but limitations in software tools prevented further progress. However, it's worth noting that the MoS_2 samples used in our work were prepared using a liquid-exfoliation method[12,13], which is known to create sufficiently low sulfur defects. Therefore, multiple factors, including the through-space spin-orbit proximity effect, collectively contribute to this unique RTP phenomenon, and the influence of each factor may vary depending on the conditions. Further studies are needed to understand these dynamics fully.

The key molecular characters to enable the through-space spin-orbit proximity effect

To open up the general applicability of the through-space spin-orbit proximity effect on POPs, we expanded the choice of TMDs and POPs in ultrafast triplet emissive heterostructure design consideration and gained insight into detailed requirements of TMDs and POPs. First, TMDs were investigated regarding the space group and the heaviness of transition metals to clarify key features of TMDs to promote the microsecond RTP of DDT. Figure 5 shows the through-space spin-orbit proximity effects of TMDs on DDT. As shown in Fig. 5a, MX_2, where M is Mo or W and X is S or Se, has 2H atomic honeycomb structures with a $P6_3/mmc$ space group. TiS_2 has a 1 T structure with a P3m1 space group. Atomic weights of Mo and W are 95.94 and 183.84, much heavier than 47.87 of Ti. For direct and consistent comparison, each TMD was transferred on a glass substrate by mechanical exfoliation, and 1 mg/ml DDT DMF solution was drop-cast on it. After solvent evaporation, the photophysical properties of the formed DDT crystals on TMD were examined. Figure 5b shows optical images of DDT crystals grown on MoS_2, $MoSe_2$, WS_2, WSe_2, and TiS_2 flakes. While green emissions were observed when the DDT crystals overlayed on MoS_2, $MoSe_2$, WS_2, and WSe_2 were excited by a focused laser beam of 365 nm, the same excitation experiment produced blue emission from the DDT on TiS_2 instead. An actual image of DDT/TMDs suspensions is shown in Supplementary Fig. 11. In Fig. 5c, it is evident that DDT on 2H-TMDs containing heavy atoms emits consistent phosphorescence around 518 nm, whereas DDT on TiS_2 generates blue fluorescence at 466 nm. In addition, the lifetime decays of DDT/TMDs are significantly differentiated into two regimes: microseconds and nanoseconds (Fig. 5d). In heavy metal-mediated 2H-TMDs, the lifetimes of DDT are 16.7, 14.2, 13.6, and 13.2 μs for MoS_2, $MoSe_2$, WS_2, and WSe_2 heterostructures, respectively. This aligns with the results of the RTP obtained from the DDT/MoS_2 interface (Figs. 2j and 3b). On the contrary, the emission decay of DDT/TiS_2 occurs within approximately 5 ns. Figure 5e presents statistical results of average emission decays extracted from 10 DDT/TMDs samples. The lifetimes of DDT crystals are 20.1 ± 1.3, 21.7 ± 2.4, 23.2 ± 1.2, and 17.6 ± 1.1 μs in combinations with MoS_2, $MoSe_2$, WS_2, and WSe_2 while DDT/TiS_2 shows nanosecond fluorescence up to 5.35 ± 0.4 ns. It is clearly shown that heavy transition metal atoms with 2H-honeycomb structures in TMDs are inevitable to enable the microsecond RTP of DDT. To assess the reproducibility of the through-space proximity spin-orbit effect of various TMDs on DDTs, we constructed DDT heterostructures using flakes obtained through mechanical exfoliation from bulk crystals but also films grown through the sulfurization of molybdenum films[58] (Supplementary Fig. 12). Our findings reliably demonstrate that microsecond-scale RTP could emerge in DDT/TMD heterostructures regardless of the specific TMDs and the crystallinity of the MoS_2 films underneath DDT crystals, as far as TMDs consist of heavy transition atoms arranged in the 2H space group.

Next, molecular design requirements of purely organic chromophores were explored to realize ultrafast triplet emission via the through-

https://doi.org/10.1038/s41467-024-51501-8

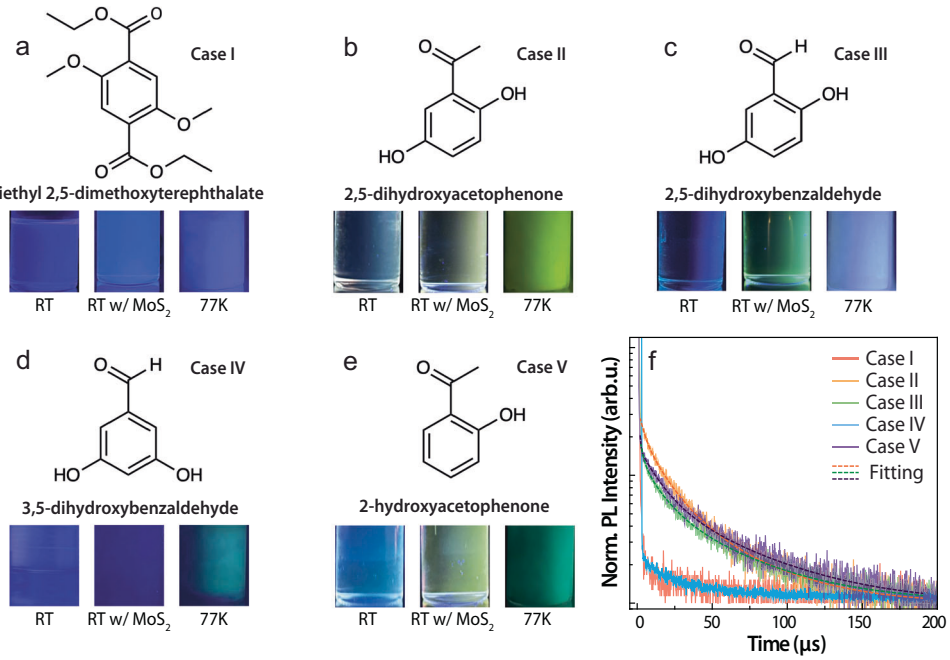

Fig. 6 | Key chemical structural features of DDT derivatives to have through-space spin-orbit proximity effect by forming rapid precipitation with MoS_2. **a**–**e** Molecular structures and dark field images of DDT derivatives at RT and 77 K and DDT derivatives/MoS_2 at RT. **f** TRPL decay spectra of the rapidly precipitated DDT derivatives with MoS_2.

space spin-orbit proximity effect of TMDs. For a clear comparison, a series of aromatic compounds were designed and synthesized to contain a carbonyl group with different side chains. Then the compounds were co-precipitated rapidly with MoS_2 in aqueous MoS_2 suspensions. Figure 6a to e present molecular structures and emission images with and without MoS_2 at RT and 77 K of DDT derivatives; diethyl 2,5-dimethoxyterephthalate, 2,5-dihydroxyacetophenone, 2,5-dihydoxybenzaldehyde, 3,5-dihydoxybenzaldehyde, and 2-hydroxyacetophenone. Supplementary Figs. 13 and 5f show the PL and TRPL spectra of DDT derivative/MoS_2 at RT.

Figure 6a presents the molecular structure of diethyl 2,5-dimethoxyterephthalate in which hydroxyl groups of DDT were replaced with methoxy side chains. However, the rapidly precipitated diethyl 2,5-dimethoxyterephthalate in the aqueous MoS_2 suspension did not show any phosphorescence emission at room temperature, suggesting that organic chromophores must have an aromatic carbonyl structure with free hydroxyl groups to rapidly form the hybrid structure with MoS_2. We then prepared 2,5-dihydroxyacetophenone to test the effectiveness of an aromatic ketone structure (Fig. 6b). This compound exhibited 19.66 μs phosphorescence emission by forming the hybrid structure with MoS_2 (Fig. 6f). Similarly, 2,5-dihydoxybenzaldehyde (Fig. 6c) also produced fast phosphorescence at 22.79 μs when in the heterostructure with MoS_2, demonstrating that the aromatic carbonyl structure works well regardless of whether it is a carboxylic acid, ketone, or aldehyde. Interestingly, we found that moving the hydroxyl group from ortho- to meta- relative to the carbonyl group prevented phosphoresce emission (Fig. 6d), indicating that the hydroxyl group must be in the ortho position to establish fast bonding with MoS_2. Finally, we discovered that the simplest structure of 2-hydroxyacetophenone shown in Fig. 6e, which contains an aromatic carbonyl with an ortho-positioned hydroxyl group, produced rapid phosphorescence emission of 25.16 μs. These results indicate that aromatic carbonyl with a free hydroxyl group at the ortho position is the essential chemical structure of organic chromophores to rapidly form strong bonding with MoS_2. The PL and TRPL decay spectra of the rapidly precipitated DDT derivatives with MoS_2 shown in Supplementary Fig. 13 and 5f clearly show that the DDT derivatives having aromatic carbonyl with ortho-hydroxyl group have microsecond phosphorescence lifetimes while the other two have nanosecond fluorescence lifetimes.

Furthermore, a new heterostructure composition of Br6A/MoS_2 was prepared to clarify the influence of TMDs on POPs already exhibiting long phosphorescence at room temperature. As reported in previous studies[13], Br6A is a purely organic compound comprising brominated aromatic aldehydes (Supplementary Fig. 14a) and has its long phosphorescent lifetime up to a millisecond regime via the heavy atom effect of halogen bonding with host molecules. Note that, unlike the above-examined organic chromophores with hydroxyl side chains, Br6A has alkoxy side chains. As anticipated, Br6A did not establish the heterostructure with MoS_2 when rapidly precipitated with MoS_2 in water, and thus no bright phosphorescence was observed. However, Br6A formed well-grown crystals on a MoS_2 flake (Supplementary Fig. 14b). As shown in Supplementary Fig. 14d, the phosphorescence lifetime of the Br6A crystal on MoS_2 was 87 μs, whereas the Br6A overhang part exhibits 1.4 ms of ultralong phosphorescence. This implies that the SOC of Br6A has a substantial boost through the through-space spin-orbit proximity effect of MoS_2, provided that MoS_2 and Br6A are in close proximity to each other.

In conclusion, our study has revealed a strategy, termed the "through-space spin-orbit proximity effect", which enables ultrafast microsecond RTP emitters by creating heterostructures of POPs and 2H-TMDs. We demonstrated that MoS_2 leverages its broken inversion symmetry and the presence of heavy atoms to alter electron spins at the carbonyl oxygens of DDT and to re-order the excited states involving (n, π*). This results in the formation of a new accessible ISC pathway and a dramatic improvement in SOCs, thereby triggering the ultrafast microsecond RTP of the DDT/MoS_2 hybrid system. We also identified the key structural features of TMDs and POPs: 2H-lattice structures with heavy transition metal atoms in TMDs and aromatic carbonyl with an ortho hydroxy in POPs. Importantly, by ensuring close spatial proximity between TMDs and POPs, the relaxation decays of POPs exhibiting slow phosphorescence can be largely improved through the through-space spin-orbit proximity effect of TMDs. This intriguing finding has significant implications, offering an approach to

design ultrafast hybrid organic triplet emitters, and holds promise for various technological advancements.

Methods

Sample preparations

All organic chromophores were purchased from Millipore Sigma and purified by recrystallization from ethanol and column chromatography with ethyl acetate and n-hexanes before investigation. Single crystals of TMDs were purchased from SPI Supplies to fabricate mechanically exfoliated TMDs using Scotch tape. Powdered TMDs were purchased from Millipore Sigma to prepare TMD suspensions by chemical exfoliation. DDT/TMDs hybrid crystals were prepared by solution drop casting method with mechanically exfoliated TMDs and 1 mg/mL in DMF or THF solution. For the hybrid suspension of organic chromophores and TMDs, a solution of organic chromophores dissolved in DMF at a concentration of 1 mg/mL was prepared by injecting 200 μL each time into distilled water with dispersed TMDs, repeated 10 times.

Characterizations

PL spectra were obtained by a laser confocal microscope (LCM) system equipped with SR-303I-B (Andor) and GF-033C-IRF (Allied vision) at λ_{ex} of 405 nm. Raman spectra were scanned by Raman spectrometer (LabRAM HR Evolution, HORIBA Co.) at λ_{ex} of 514 nm. Time-correlated single photon counting (TCSPC) and time-resolved photoluminescence (TRPL) were used to characterize the lifetime profiles with impulse response function full-width half maximum of 240 ps at λ_{ex} of 375 nm. The lattice structure of single organic crystals was analyzed by SCXRD at the atomic scale. EPR analysis was carried out with a JES-FA200 (JEOL) CW EPR spectrometer (F_q100.00, md1.0, am1.00 × 100, tc0.03) with a sweep time of 60 s at X band frequency of up to 9.4 GHz under dark and light conditions. L-EPR measurement utilized a 375 nm laser with an incident power of 16 mW. For room temperature EPR measurements, the DDT/MoS_2 solution was freeze-dried in a powder form.

DFT calculation

For optimizing the DDT and DDT/MoS_2 crystal structure coordination, the vdW-corrected DFT calculations were performed using the double-zeta plus polarization (DZP) basis set in the SIESTA package[59,60]. The local-density approximation (LDA)[61] and generalized gradient approximations (GGA) of Perdew-Burke-Ernzerhof (PBE) were used as exchange-correlation potentials[62]. The vdW interaction was applied with an exchange-correlation function (i.e. DRSLL)[62]. These calculations were performed under spin-unpolarized conditions. The energy cut-off was set at 300 Ry, and only the gamma-point mesh was performed. The atomic coordinates were optimized by using the conjugate gradient method with a maximum force tolerance of 0.01 eV/Å in the absence of an electric field. The DDT/MoS_2 structure information before the structure-optimization was modeled based on the SCXRD experiment. The DDT structure information was given to the Cambridge Crystallographic Data Center (CCDC) reference number 128054 via www.ccdc.cam.ac.uk. Detailed structure information is described in the supplementary information as Fig. S7.

Additional quantum chemical computations were performed using the Q-Chem 5.2 software package[63]. For these (higher-level) simulations, the MoS_2 surface is truncated to a single Mo unit, containing the six proximate S atoms and 12 additional hydrogen atoms to close the covalent bonds of the S. In the optimization step, the Mo and S atoms were fixed in position, and the hydrogen atoms were relaxed. The ground-state geometries of DDT and single-unit MoS_2 were obtained by density functional theory (DFT), using the B3LYP functional[64], together with the polarized def2-SV(P) basis set[65,66]. Optimization of the lowest energy triplet state (T_1) was performed using unrestricted DFT, and that of the ground state (S_0) was performed using the restricted DFT. Excited state simulations were performed using time-dependent DFT (TD-DFT) within the Tamm-Dancoff approximation (TDA)[67]. Single-point energy calculations, of both the DDT molecule and the DDT/MoS_2 surface, were also conducted using the B3LYP functional[64], together with the polarized def2-SV(P) basis set[65,66]. Characters of excitations were described with natural transition orbitals (NTOs)[68]. The ground state singlet (S_0) geometry was used to calculate spin–orbit coupling (SOC) constants[69,70] within TD-DFT. Natural transition orbitals (NTOs) of TD-DFT calculations were visualized using IQMOL.

Data availability

The datasets generated and analyzed during the current study are available from the corresponding author on request.

References

1. Mukherjee, S. & Thilagar, P. Recent advances in purely organic phosphorescent materials. *Chem. Commun.* **51**, 10988–11003 (2015).
2. Shao, W. & Kim, J. Metal-free organic phosphors toward fast and efficient room-temperature phosphorescence. *Acc. Chem. Res.* **55**, 1573–1585 (2022).
3. Maldiney, T. et al. The in vivo activation of persistent nanophosphors for optical imaging of vascularization, tumours and grafted cells. *Nat. Mater.* **13**, 418–426 (2014).
4. Zhang, G., Palmer, G. M., Dewhirst, M. W. & Fraser, C. L. A dual-emissive-materials design concept enables tumour hypoxia imaging. *Nat. Mater.* **8**, 747–751 (2009).
5. Kang, D. H., Zeng, Y., Tewari, M. & Kim, J. Highly sensitive and quantitative biodetection with lipid-polymer hybrid nanoparticles having organic room-temperature phosphorescence. *Biosens. Bioelectron.* **199**, 113889 (2022).
6. Zeng, Y. et al. Chorioretinal hypoxia detection using lipid-polymer hybrid organic room-temperature phosphorescent nanoparticles. *ACS Appl. Mater. Interfaces* **14**, 18182–18193 (2022).
7. Wang, Q. H., Kalantar-Zadeh, K., Kis, A., Coleman, J. N. & Strano, M. S. Electronics and optoelectronics of two-dimensional transition metal dichalcogenides. *Nat. Nanotechnol.* **7**, 699–712 (2012).
8. Yu, Y. et al. Room-temperature-phosphorescence-based dissolved oxygen detection by core-shell polymer nanoparticles containing metal-free organic phosphors. *Angew. Chem. Int.* **56**, 16207–16211 (2017).
9. An, Z. et al. Stabilizing triplet excited states for ultralong organic phosphorescence. *Nat. Mater.* **14**, 685–690 (2015).
10. Gu, L. et al. Colour-tunable ultra-long organic phosphorescence of a single-component molecular crystal. *Nat. Photonics* **13**, 406–411 (2019).
11. Song, B., Shao, W., Jung, J., Yoon, S.-J. & Kim, J. Organic light-emitting diode employing metal-free organic phosphor. *ACS Appl. Mater. Interfaces* **12**, 6137–6143 (2020).
12. Lee, D. R. et al. Heavy atom effect of selenium for metal-free phosphorescent light-emitting diodes. *Chem. Mater.* **32**, 2583–2592 (2020).
13. Bolton, O., Lee, K., Kim, H.-J., Lin, K. Y. & Kim, J. Activating efficient phosphorescence from purely organic materials by crystal design. *Nat. Chem.* **3**, 205–210 (2011).
14. Zhao, W. et al. Rational molecular design for achieving persistent and efficient pure organic room-temperature phosphorescence. *Chem* **1**, 592–602 (2016).
15. He, Z. et al. White light emission from a single organic molecule with dual phosphorescence at room temperature. *Nat. Commun.* **8**, 416 (2017).
16. Cai, S. et al. Enabling long-lived organic room temperature phosphorescence in polymers by subunit interlocking. *Nat. Commun.* **10**, 4247 (2019).

17. Bolton, O., Lee, D., Jung, J. & Kim, J. Tuning the photophysical properties of metal-free room temperature organic phosphors via compositional variations in bromobenzaldehyde/dibromobenzene mixed crystals. *Chem. Mater.* **26**, 6644–6649 (2014).
18. Kwon, M. S. et al. Suppressing molecular motions for enhanced room-temperature phosphorescence of metal-free organic materials. *Nat. Commun.* **6**, 8947 (2015).
19. Lee, D. et al. Room temperature phosphorescence of metal-free organic materials in amorphous. *Polym. Matrices J. Am. Chem. Soc.* **135**, 6325–6329 (2013).
20. Zang, L., Shao, W., Kwon, M. S., Zhang, Z. & Kim, J. Photoresponsive luminescence switching of metal-free organic phosphors doped polymer matrices. *Adv. Opt. Mater.* **8**, 2000654 (2020).
21. Arunkumar, S., Ghosh, D. & Kumar, G. R. Heavy main group element containing organometallic phosphorescent materials. *Results Chem.* **4**, 100399 (2022).
22. Baba, M. Intersystem Crossing in the 1 nπ* and 1 ππ* States. *J. Phys. Chem. A* **115**, 9514–9519 (2011).
23. Gmitra, M. & Fabian, J. Graphene on transition-metal dichalcogenides: A platform for proximity spin-orbit physics and optospintronics. *Phys. Rev. B* **92**, 155403 (2015).
24. Avsar, A. et al. Spin–orbit proximity effect in graphene. *Nat. Commun.* **5**, 4875 (2014).
25. Wang, Z. et al. Strong interface-induced spin–orbit interaction in graphene on WS2. *Nat. Commun.* **6**, 8339 (2015).
26. Cho, E. et al. A single-benzene-based fluorophore: optical waveguiding in the crystal form. *Chempluschem* **84**, 1130–1134 (2019).
27. Gurarslan, A. et al. Van der Waals Force Isolation of Monolayer MoS 2. *Adv. Mater.* **28**, 10055–10060 (2016).
28. Bulliard, X. et al. Enhanced Performance in Polymer Solar Cells by Surface Energy Control. *Adv. Funct. Mater.* **20**, 4381–4387 (2010).
29. Sawicki, E. & Johnson, H. Characterization of aromatic compounds by low-temperature fluorescence and phosphorescence: application to air pollution studies. *Microchem. J.* **8**, 85–101 (1964).
30. Kearns, D. R. & Case, W. A. Investigation of singlet → triplet transitions by the phosphorescence excitation method. iii. aromatic ketones and aldehydes. *J. Am. Chem. Soc.* **88**, 5087–5097 (1966).
31. Ma, H. et al. Hydrogen bonding-induced morphology dependence of long-lived organic room-temperature phosphorescence: a computational study. *J. Phys. Chem. Lett.* **10**, 6948–6954 (2019).
32. Ma, H. et al. Electrostatic interaction-induced room-temperature phosphorescence in pure organic molecules from qm/mm calculations. *J. Phys. Chem. Lett.* **7**, 2893–2898 (2016).
33. Singh, A. K. et al. 2D layered transition metal dichalcogenides (MoS2): Synthesis, applications and theoretical aspects. *Appl. Mater. Today* **13**, 242–270 (2018).
34. Silbernagel, B. G. Electron spin resonance of sulfide catalysts. *J. Magn. Magn. Mater.* **31–34**, 885–886 (1983).
35. Panich, A. M., Shames, A. I., Rosentsveig, R. & Tenne, R. A magnetic resonance study of MoS 2 fullerene-like nanoparticles. *J. Phys. Condens. Matter* **21**, 395301 (2009).
36. Yin, Y. et al. Contributions of phase, sulfur vacancies, and edges to the hydrogen evolution reaction catalytic activity of porous molybdenum disulfide nanosheets. *J. Am. Chem. Soc.* **138**, 7965–7972 (2016).
37. González, J. R., Alcántara, R., Tirado, J. L., Fielding, A. J. & Dryfe, R. A. W. Electrochemical interaction of few-layer molybdenum disulfide composites vs sodium: new insights on the reaction mechanism. *Chem. Mater.* **29**, 5886–5895 (2017).
38. Svorec, J. et al. Determination of intermolecular copper–copper distances from the EPR half-field transitions and their comparison with distances from X-ray structures: applications to copper(II) complexes with biologically important ligands. *Transit. Met. Chem.* **34**, 129–134 (2009).
39. Toledo, J. R. et al. Electron paramagnetic resonance signature of point defects in neutron-irradiated hexagonal boron nitride. *Phys. Rev. B* **98**, 155203 (2018).
40. Schott, S. et al. Tuning the effective spin-orbit coupling in molecular semiconductors. *Nat. Commun.* **8**, 15200 (2017).
41. Tait, C. E. et al. Reveals triplet state delocalization in a series of cyclic and linear π-conjugated porphyrin oligomers. *J. Am. Chem. Soc.* **137**, 8284–8293 (2015).
42. Stevenson, R. Triplet state EPR spectra. *J. Magn. Reson.* **57**, 24–42 (1984).
43. Cameron, T. S. et al. Characterisation of the thermally accessible spin triplet state in dimers of the 7π ClCNSSS+. in the solid state. *Chem. Commun.* 2277 https://doi.org/10.1039/b602843h (2006).
44. Richert, S., Tait, C. E. & Timmel, C. R. Delocalisation of photoexcited triplet states probed by transient EPR and hyperfine spectroscopy. *J. Magn. Reson.* **280**, 103–116 (2017).
45. Atsarkin, V. A., Demidov, V. V., Vasneva, G. A. & Gotovtsev, D. G. Electron spin resonance and longitudinal relaxation around phase transition in La0.9Ca0.1 MnO3. *Appl. Magn. Reson.* **21**, 147–156 (2001).
46. Krbal, M. et al. Improved ordering of quasi-two-dimensional mos 2 via an amorphous-to-crystal transition initiated from amorphous sulfur-rich MoS 2+ x. *Cryst. Growth Des.* **22**, 3072–3079 (2022).
47. Gottscholl, A. et al. Initialization and read-out of intrinsic spin defects in a van der Waals crystal at room temperature. *Nat. Mater.* **19**, 540–545 (2020).
48. Closs, G. L., Forbes, M. D. E. & Piotrowiak, P. Spin and reaction dynamics in flexible polymethylene biradicals as studied by EPR, NMR, optical spectroscopy, and magnetic field effects. Measurements and mechanisms of scalar electron spin-spin coupling. *J. Am. Chem. Soc.* **114**, 3285–3294 (1992).
49. Niklas, J. et al. Photoinduced dynamics of charge separation: from photosynthesis to polymer–fullerene bulk heterojunctions. *J. Phys. Chem. B* **119**, 7407–7416 (2015).
50. Moses, P. G., Mortensen, J. J., Lundqvist, B. I. & Nørskov, J. K. Density functional study of the adsorption and van der Waals binding of aromatic and conjugated compounds on the basal plane of MoS2. *J. Chem. Phys.* **130**, 104709 (2009).
51. Patil, U. & Caffrey, N. M. Adsorption of common solvent molecules on graphene and MoS 2 from first-principles. *J. Chem. Phys.* **149**, 094702 (2018).
52. Guan, G. et al. Protein induces layer-by-layer exfoliation of transition metal dichalcogenides. *J. Am. Chem. Soc.* **137**, 6152–6155 (2015).
53. Amani, M. et al. High luminescence efficiency in mos 2 grown by chemical vapor deposition. *ACS Nano* **10**, 6535–6541 (2016).
54. Shao, W., Jiang, H., Ansari, R., Zimmerman, P. M. & Kim, J. Heavy atom oriented orbital angular momentum manipulation in metal-free organic phosphors. *Chem. Sci.* **13**, 789–797 (2022).
55. Xiao, D., Liu, G.-B., Feng, W., Xu, X. & Yao, W. Coupled spin and valley physics in monolayers of mos2 and other group-vi dichalcogenides. *Phys. Rev. Lett.* **108**, 196802 (2012).
56. Hong, J. et al. Exploring atomic defects in molybdenum disulphide monolayers. *Nat. Commun.* **6**, 6293 (2015).
57. Tsai, J.-Y., Pan, J., Lin, H., Bansil, A. & Yan, Q. Antisite defect qubits in monolayer transition metal dichalcogenides. *Nat. Commun.* **13**, 492 (2022).
58. Im, H. et al. Chaotic organic crystal phosphorescent patterns for physical unclonable functions. *Adv. Mater.* **33**, 2102542 (2021).
59. García, A. et al. Siesta: Recent developments and applications. *J. Chem. Phys.* **152**, 204108 (2020).
60. Dion, M., Rydberg, H., Schröder, E., Langreth, D. C. & Lundqvist, B. I. Van der Waals Density Functional for General Geometries. *Phys. Rev. Lett.* **92**, 246401 (2004).
61. Perdew, J. P. & Zunger, A. Self-interaction correction to density-functional approximations for many-electron systems. *Phys. Rev. B* **23**, 5048–5079 (1981).

62. Perdew, J. P., Burke, K. & Ernzerhof, M. Generalized gradient approximation made simple. *Phys. Rev. Lett.* **77**, 3865–3868 (1996).
63. Shao, Y. et al. Advances in molecular quantum chemistry contained in the Q-Chem 4 program package. *Mol. Phys.* **113**, 184–215 (2015).
64. Lee, C., Yang, W. & Parr, R. G. Development of the Colle-Salvetti correlation-energy formula into a functional of the electron density. *Phys. Rev. B* **37**, 785–789 (1988).
65. Weigend, F. & Ahlrichs, R. Balanced basis sets of split valence, triple zeta valence and quadruple zeta valence quality for H to Rn: Design and assessment of accuracy. *Phys. Chem. Chem. Phys.* **7**, 3297 (2005).
66. Weigend, F. Accurate Coulomb-fitting basis sets for H to Rn. *Phys. Chem. Chem. Phys.* **8**, 1057 (2006).
67. Hirata, S. & Head-Gordon, M. Time-dependent density functional theory within the Tamm–Dancoff approximation. *Chem. Phys. Lett.* **314**, 291–299 (1999).
68. Martin, R. L. Natural transition orbitals. *J. Chem. Phys.* **118**, 4775–4777 (2003).
69. Samanta, P. K., Kim, D., Coropceanu, V. & Brédas, J.-L. Up-conversion intersystem crossing rates in organic emitters for thermally activated delayed fluorescence: impact of the nature of singlet vs triplet. *Excited S. J. Am. Chem. Soc.* **139**, 4042–4051 (2017).
70. Beljonne, D., Shuai, Z., Pourtois, G. & Bredas, J. L. Spin–orbit coupling and intersystem crossing in conjugated polymers: a configuration interaction description. *J. Phys. Chem. A* **105**, 3899–3907 (2001).

Acknowledgements

This work was supported by the National Research Foundation of Korea (NRF) grant, funded by the Korea government (MSIT) (RS-2024-00357783; D. H. Park) and the START grant from the College of Engineering of the University of Michigan (J. Kim). This research was supported by the National Research Foundation of Korea (2021M3H4A1A02056037; S. Kim and RS-2024-00448809; S. Kim) and the BrainLink program, funded by the Ministry of Science and ICT through the National Research Foundation of Korea (RS-2023-00237308; S. Kim).

Author contributions

J.C. and H.I. contributed equally by preparing all materials, obtaining experimental data, and analyzing the results. J.K., S.K. and D.H.P. conceived and directed this project. J.C. and J-M.H. conducted a study on the synthesis of organic molecules and analyzed their photophysical properties. D.W.K., G.W.J. and J.W.J. performed the EPR experiment and the DFT calculation of DDT assembly on MoS_2, and analyzed the results. H.J., A.S., W.S. and P.Z. performed the quantum chemical computations. E.H.W. provided constructive opinions and suggestions for DFT calculations. All the authors discussed and contributed to the results. H.I., J.C. and J.K. drafted the manuscript. All the authors have approved the final version of the manuscript.

Competing interests

The authors declare no competing interests.

Additional information

Supplementary information The online version contains supplementary material available at https://doi.org/10.1038/s41467-024-51501-8.

Correspondence and requests for materials should be addressed to Sunkook Kim, Dong Hyuk Park or Jinsang Kim.

Peer review information *Nature Communications* thanks the anonymous reviewer(s) for their contribution to the peer review of this work. A peer review file is available.